IOPscience iopscience.iop.org

Home Search Collections Journals About Contact us My IOPscience

The structure of hexane/perfluorohexane thin liquid films

This article has been downloaded from IOPscience. Please scroll down to see the full text article.

2001 J. Phys.: Condens. Matter 13 4957

(http://iopscience.iop.org/0953-8984/13/21/321)

View the table of contents for this issue, or go to the journal homepage for more

Download details:
IP Address: 171.66.16.226
The article was downloaded on 16/05/2010 at 13:23

Please note that terms and conditions apply.

INSTITUTE OF PHYSICS PUBLISHING JOURNAL OF PHYSICS: CONDENSED MATTER

J. Phys.: Condens. Matter **13** (2001) 4957–4972 www.iop.org/Journals/cm PII: S0953-8984(01)19834-6

The structure of hexane/perfluorohexane thin liquid films

W Prange, T Kurbjuhn, M Tolan and W Press

Institut für Experimentelle und Angewandte Physik, Christian-Albrechts-Universität Kiel, Leibnizstraße 17–19, 24098 Kiel, Germany

Received 6 December 2000

Abstract

Thin films of the binary liquid mixture hexane/perfluorohexane were prepared on silicon wafers. The film thicknesses were between 140 Å and 350 Å; this range was chosen in order to achieve strong confinement of the mixture. The vertical structure of these films was investigated by means of x-ray reflectivity measurements. The data show that the component with the lower surface tension (perfluorohexane) segregates in the surface region of the films in agreement with theoretical predictions. Furthermore, no complete miscibility of the two components was observed in regions of the phase diagram where a one-component bulk system is expected. Preliminary results are given for the internal hexane/perfluorohexane interface.

1. Introduction

The investigation of thin liquid films has attracted great attention in the past. Thin liquid films are systems where the molecules are trapped between the solid/liquid and the liquid/gas interfaces. The confinement of a liquid by a 'wall' is expected to alter the structure drastically. While there have been many theoretical investigations on this topic (see e.g. [1–9] and references therein) only few experimental studies exist. These experiments have shed light on the atomic structure of the solid/liquid [10–15] and the liquid/gas interface [16,17], respectively. In the latter case layering effects have been observed for metallic liquids such as mercury, gallium, and indium induced by the presence of the free surface which is here acting as the 'hard wall'. The former studies yielded evidence for layering of gallium and tetrakis(2-ethylhexoxy)silane next to diamond and silicon surfaces, respectively. Furthermore layering was also found in liquid cyclohexane films while a pronounced low-density region was observed for liquid hexane films on silicon substrates [12–15]. These studies have shown that density fluctuations within a thin liquid film are highly sensitive to the shape of the molecules of non-polar van der Waals liquids.

So far only studies of one-component liquids have been mentioned. In the last few decades the properties of binary liquids have been extensively investigated both experimentally and theoretically. Here the experiments have concentrated on the bulk properties and the determination of phase diagrams of such systems [18, 19]. Many interesting and universal

 © 2001 IOP Publishing Ltd Printed in the UK

properties have been found where the so-called critical adsorption or the bulk interface is the most prominent feature [20–29]. However, to our knowledge only one study exists so far where the properties of binary liquids confined in a thin-film geometry were directly investigated with ångström resolution [30]. The study presented in reference [31] finds indirect evidence of structural properties of binary liquid films from ellipsometric measurements.

This article presents a detailed study of the microscopic structure of thin liquid films consisting of hexane/perfluorohexane mixtures. The thicknesses d of the films were between $d = 140$ Å and $d = 350$ Å. The bulk phase diagram of hexane/perfluorohexane mixtures is well known and shows a miscibility gap with an upper critical solution temperature near $T = 295$ K [29, 32].

Since liquids cannot be investigated by direct probes such as AFM or STM, scattering techniques are mandatory. The vertical structure of the films was determined on an ångström scale by means of x-ray reflectivity. This technique has been successfully applied to investigate the electron-density profiles of many thin-film materials (see references [33, 34] and references therein). It is in particular well suited for use in the study of 'soft' materials such as polymers and liquids [35].

The article is organized as follows. First the microscopic properties of the two liquids and the bulk properties of the binary system hexane/perfluorohexane are described. In the next section the theory which is used in order to explain the x-ray reflectivity data will be discussed. We concentrate here on a data inversion technique that helps to highlight small features in electron-density profiles. The experimental set-up and the sample preparation will be presented in the following section. The final section deals with the measurements and the discussion of the results while conclusions and an outlook are given at the end of this article.

2. The hexane/perfluorohexane system

Mixtures of the van der Waals liquids n-hexane (purchased from Fluka Chemika; 99.5% purity) and perfluorohexane (purchased from Sigma-Aldrich Chemie; purity of at least 99%) were used for the experiments. For each series of x-ray experiments an amount between 1.2 and 2.0 ml was prepared. As substrates, polished silicon (100) wafers of size 20 mm $\times$ 20 mm (provided by Wacker Siltronic) were used for each series of measurements. After cleaning by heating for 10 min at 80 °C in a 5:1:1 mixture of deionized water, 30% concentrated NaOH, and 30% concentrated H_2O_2 solution and subsequent rinsing with deionized water, very smooth substrates with a native oxide layer of thickness $d_{ox} \approx 10$ Å–15 Å and a surface roughness of $\sigma \sim 2$ Å–3 Å were obtained[1]. This was determined by measuring the x-ray reflectivity of the bare substrates. The diffuse scattering from the substrates is negligible, indicating smooth surfaces. Further, atomic force microscopy has directly shown that this cleaning procedure leads to very smooth and uniform surfaces.

The n-hexane and perfluorohexane molecules have pencil-like elongated shape with main diameter $\sim$5 Å and length $\sim$11 Å. Perfluorohexane is a 'stiff rod' with almost no configurational freedom in contrast to the flexible n-hexane molecules. The melting points of hexane and perfluorohexane are $T_{m,hex} = 178$ K and $T_{m,per} = 186$ K, the surface tensions are $\gamma_{hex} = 17.9$ mN m^{-1} and $\gamma_{per} = 12.0$ mN m^{-1}, and the densities are $\rho_{hex} = 0.655$ g cm^{-3} and $\rho_{per} = 1.70$ g cm^{-3}, respectively [36]. Since the density contrast between the two materials is rather large, they are well suited for use in x-ray studies of mixing behaviour. Bulk mixtures of hexane and perfluorohexane were found to exhibit a consolute point at $T_c = 295.2$ K

[1] The Si/SiO_2 interface was determined by means of specular reflectivity, too.

with a critical density of $\rho_c = 1.14$ g cm^{-3} [29, 32]. This corresponds to a volume ratio of approximately 1:1—that is, to a perfluorohexane concentration of $c_{\rm p.f.} = 0.5$.

McClain *et al* [29] found from x-ray transmission measurements that in the (ρ, T) bulk phase diagram of hexane/perfluorohexane mixtures, the one-phase region where a mixture of the two materials exists and the coexistence regime with two phases are separated by a line given by $\rho(t) = \rho_c(1 \pm 0.5At^{\beta} + Ct^{1-\alpha})$ where $t = (T_c - T)/T$ is the reduced temperature, $\alpha = 0.11$ and $\beta = 0.32$ are the specific heat and order parameter exponents of the 3D Ising model, and $A = 1.899$ and $C = 0.51$ are fitting parameters [29]. In this article we will address to what extent the bulk phase diagram can be applied to thin films of hexane/perfluorohexane mixtures.

3. X-ray reflectivity

X-ray reflectivity may be discussed in terms of a purely optical language. The reflectivity of a single surface is given by the well-known Fresnel formulae [37]. The only difference from conventional optics is that the real part of the refractive index n for x-rays is slightly smaller than unity, i.e. $n = 1 - \delta + i\beta$, where the dispersion δ is positive and proportional to the electron-density ϱ of the material and β accounts for absorption. The reflectivity for arbitrary electron-density profiles $\varrho(z)$ may be calculated by slicing such a profile into very thin slabs of constant density and calculating the reflected intensity from these slabs via the famous Parratt iteration [38] or, equivalently, the matrix method introduced earlier by Abelès [39].

The Parratt algorithm considers scattering from several sharp interfaces. If a density profile $\varrho(z)$ is sliced into many very thin layers, then this technique provides a simple approach for the calculation of the reflectivity from an arbitrary system. Figure 1 shows schematically a layer system consisting of N interfaces at positions $z_j \leqslant 0$. The vacuum counts as 'layer 1'

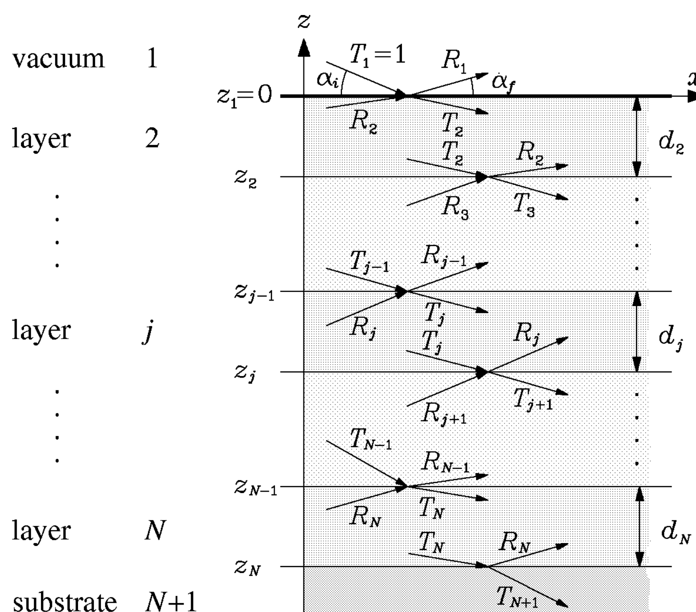

Figure 1. A sketch of a system consisting of $N + 1$ layers with N interfaces. In the case of specular reflectivity the condition $\alpha_i = \alpha_f$ holds. The incident wave amplitude is normalized to unity, $T_1 = 1$. No wave is reflected from the bottom of the substrate, i.e. $R_{N+1} = 0$.

with the first interface at $z_1 = 0$. The last interface is located at z_N, together with the underlying semi-infinite substrate ('layer $N + 1$'). The refractive index of each layer with thickness $d_j = z_{j-1} - z_j$ is denoted by $n_j = 1 - \delta_j + i\beta_j$; $\vec{k}_{i,j}$ and T_j are the wavevector and the amplitude of the transmitted wave and $\vec{k}_{f,j}$ and R_j are the corresponding values for the reflected wave inside layer j. The impinging wave with an amplitude normalized to unity, $T_1 = 1$, hits the surface at the grazing angle α_i. In what follows, we will show how the amplitude R_1 of the specularly reflected wave may be calculated. If X_{j+1} denotes the ratio of R_{j+1} and T_{j+1} in layer $j + 1$, then X_j for the layer above may be calculated via [38]

$$X_j = \frac{R_j}{T_j} = \exp(-2ik_{z,j}z_j)\frac{r_{j,j+1} + X_{j+1}\exp(2ik_{z,j+1}z_j)}{1 + r_{j,j+1}X_{j+1}\exp(2ik_{z,j+1}z_j)} \tag{1}$$

where

$$r_{j,j+1} = \frac{k_{z,j} - k_{z,j+1}}{k_{z,j} + k_{z,j+1}} \tag{2}$$

is the Fresnel coefficient of interface j with $k_{z,j} = k(n_j^2 - \cos^2\alpha_i)^{1/2}$ being the z-component of the wavevector in layer j [37]. In general, the substrate is much thicker than the penetration depth of x-rays. Consequently there is no reflection from the bottom of the substrate, i.e. one may set $R_{N+1} = X_{N+1} = 0$ at the start of the recursion. The specularly reflected intensity R is obtained from equation (1) after N iterations:

$$R = |X_1|^2 = |R_1|^2. \tag{3}$$

As an example, figure 2 shows the calculated specular reflectivity for a hexane/perfluorohexane thin liquid film of thickness $d = 296$ Å on a silicon substrate quite similar to those which will be discussed below. The parameters used in the calculation are the wavelength $\lambda = 0.83$ Å, and $\delta_{\text{Si}} = 2.16 \times 10^{-6}$, $\beta_{\text{Si}}/\delta_{\text{Si}} = 1/147$. The calculation was done by treating the film as a homogeneous 1:1 by volume mixture of the two liquids with the parameters $\delta_{\text{hex}} = 0.71 \times 10^{-6}$, $\beta_{\text{hex}}/\delta_{\text{hex}} = 1/3600$, and $\delta_{\text{p.f.}} = 1.49 \times 10^{-6}$, $\beta_{\text{p.f.}}/\delta_{\text{p.f.}} = 1/750$.

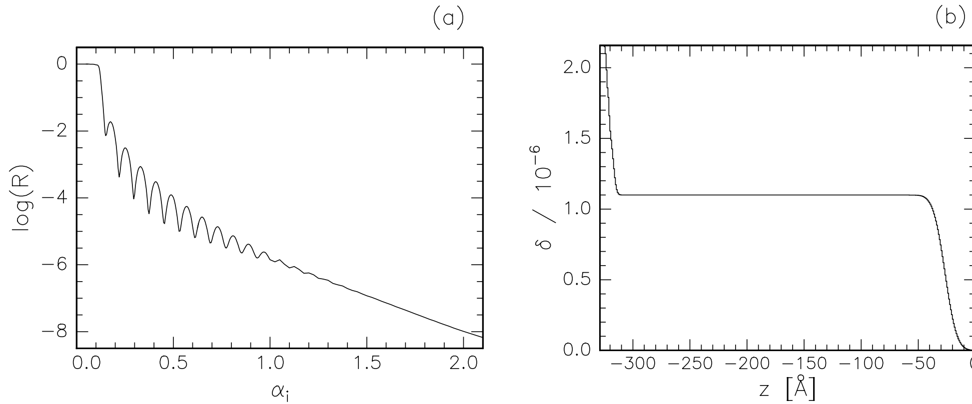

Figure 2. An example of a calculated reflectivity (a) of a homogeneous film with dispersion $\delta = 1.1 \times 10^{-6}$ on a Si substrate with $\delta_{\text{Si}} = 2.16 \times 10^{-6}$ (b). The Kiessing fringes in the reflectivity indicate a film thickness $d = 296$ Å.

The reflectivity is unity for small angles of incidence $\alpha_i < \alpha_c$ with $\alpha_c = \sqrt{2\delta} \sim 0.1^\circ{-}0.4^\circ$ the critical angle of total reflection. The penetration depth of 15 keV x-rays is limited to approximately 50 Å in this region of total external reflection. For larger incident angles, $\alpha_i > \alpha_c$, the reflectivity decreases rapidly with $(\alpha_c/2\alpha_i)^4$, but with oscillations superimposed

(so-called 'Kiessing fringes'). These oscillations stem from interferences of the reflected waves at the different interfaces in the system. From the period $\Delta\alpha_{\rm i}$ of these fringes the total layer thickness may be estimated via

$$d = 2\pi/\Delta q_z \approx \lambda/(2\,\Delta\alpha_{\rm i})$$

where $q_z = 2k\sin\alpha_{\rm i}$ is the z-component of the wavevector transfer $\vec{q} = \vec{k}_{\rm f} - \vec{k}_{\rm i}$ in vacuum.

In order to determine the density profile from x-ray reflectivity data it is common to describe a profile by a few parameters: the layer thicknesses, the electron densities, and the roughnesses. Using these parameters a reflectivity curve is calculated via the Parratt formalism (see above). The parameters are varied in a least-squares fitting algorithm to minimize the difference between the calculated and measured reflectivity. The advantage of this procedure is that just a few parameters are sufficient to describe a layer system. However, often tiny features of a density profile which may hardly be described by a layer structure are expected. Then another technique of data analysis is preferred which has been developed in the last few years, namely data inversion [40–44].

The principle of inversion techniques may be discussed using a different description which is more common in the x-ray scattering community: the kinematical or first-order Born approximation. The kinematical approximation allows a clearer treatment of the scattering, from which general conclusions may be more easily drawn. In the kinematical or 'weak-scattering' limit the cross section is proportional to the Fourier transform of the total three-dimensional electron density $\varrho(x, y, z)$ of the scatterer. For surfaces this can be reformulated, and the following expression results [45, 46]:

$$R(q_z) = R_{\rm F}(q_z)\left|\frac{1}{\varrho_\infty}\int \frac{{\rm d}\varrho(z)}{{\rm d}z}\exp(-{\rm i}q_z z)\,{\rm d}z\right|^2 = R_{\rm F}(q_z)\left|F(q_z)\right|^2 \tag{4}$$

for the reflectivity $R(q_z)$. Here q_z again denotes the vertical wavevector transfer, $\varrho(z)$ is the laterally averaged electron-density profile, and ϱ_∞ is the average density of the substrate. The pre-factor $R_{\rm F}(q_z)$ is the usual Fresnel reflectivity of the substrate (see equation (2)). It is worth noting that the structure factor $F(q_z)$ is associated with the derivative of the density profile ${\rm d}\varrho(z)/{\rm d}z$ by a simple one-dimensional Fourier transform. The inversion of this Fourier transform yields a density–density correlation function (1D Patterson function) which may be directly related to vertical length scales of the system under consideration [11]. It has been shown that the sensitivity of this approach may be improved considerably by special truncation, i.e. filter techniques [46]. Particularly for low-contrast systems, transformation to real space may enhance features which would otherwise remain invisible.

However, the way in which most of the data which will be presented in this article have been analysed is different again. We have used a direct data inversion by using a phase approximation of the structure factor $F(q_z)$. Equation (4) shows that only the modulus can be directly obtained from a reflectivity measurement. The lack of phase information may lead to ambiguities in the data interpretation. Recently, the feasibility of using phase approximations based on pre-knowledge of a system has been shown [44].

In order to invert reflectivity data, a start profile $\varrho_0(z)$ which contains the pre-information that is available for the system (estimated layer thicknesses, mean layer densities, number of layers, etc) is needed. Then the difference between this profile and the unknown profile $\varrho(z)$ is given by

$$\Delta\varrho(z) = \varrho(z) - \varrho_0(z). \tag{5}$$

In what follows, $F_0(q_z)$ denotes the (known) 1D structure factor corresponding to $\varrho_0(z)$ as defined by equation (4) and $\Delta\tilde{\varrho}(q_z)$ is the (unknown) Fourier transform of $\Delta\varrho(z)$.

After some algebra the following equation for the density difference between the known start profile and the unknown electron-density profile of the sample may be found:

$$\Delta\tilde{\varrho}(q_z) = \frac{\mathrm{i}\varrho_\infty}{q_z}\left[\left|F_0(q_z)\right| - \sqrt{\frac{R(q_z)}{R_F(q_z)}}\exp\{\mathrm{i}\,\Delta\Phi(q_z)\}\right]\exp\{\mathrm{i}\Phi_0(q_z)\} \qquad (6)$$

with $\Phi(q_z)$ and $\Phi_0(q_z)$ the phases of the structure factors $F(q_z)$ and $F_0(q_z)$, respectively, and the phase difference $\Delta\Phi(q_z) = \Phi(q_z) - \Phi_0(q_z)$. Equation (6) is well suited for applying a phase approximation [44]. The simplest approximation of the phase difference is given by setting $\Delta\Phi(q_z) \equiv 0$. This means that the phases of the start profile and of the unknown profile already coincide very well. This approximation already yields good results. Other types of phase approximation may be found in reference [44].

We have generated the start profiles $\varrho_0(z)$ by conventional fitting of the data on the basis of the Parratt algorithm as discussed before (see equations (1)–(3)). A subsequent refinement followed the fitting procedure, where equation (6) was used in an iterative way. This means that the resulting profile after applying equation (6) was used as the new starting profile $\varrho_0(z)$ for the inversion. This procedure was repeated until the differences between the respective start profile and that resulting from the inversion became negligible.

The dispersion δ and the absorption β of the refractive index n are both proportional to the electron density ϱ. Hence, a dispersion profile $\delta(z)$ has essentially the same properties as the corresponding density profile $\varrho(z)$. Therefore in the measurements section, only dispersion profiles are mentioned.

4. Experimental set-up and sample preparation

The x-ray reflectivity experiments were carried out at the beamline D4.1 at HASYLAB (DESY Hamburg). The resolution defined by the slit widths was $\delta_{q_z} \approx 2 \times 10^{-3}$ Å^{-1} where q_z denotes the component of the scattering vector $\vec{q} = \vec{k}_\mathrm{f} - \vec{k}_\mathrm{i}$ perpendicular to the sample surface. The other directions are of no importance for reflectivity measurements. The scattering geometry is sketched in figure 3. The measurements were performed with a photon energy of 15 keV ($\lambda = 0.83$ Å). It should be noted that in strong contrast to the case for measurements of the x-ray reflectivity from bulk liquid surfaces, here the background may be determined by a simple off-specular scan and subtracted, since essentially no bulk scattering is present, even for the thickest films of $d \sim 350$ Å. This is confirmed by a detailed analysis of the diffuse scattering which shows that in a transverse scan, a resolution-limited specular peak riding on a broad diffuse signal is always observed [12, 47]. Furthermore, it is worth mentioning that the liquid films were in equilibrium with the respective vapour inside the sample cell. Thus isotropic background scattering is caused which depends on the vapour pressure of the materials. This is essentially why some reflectivities could be measured to larger q_z-values than others.

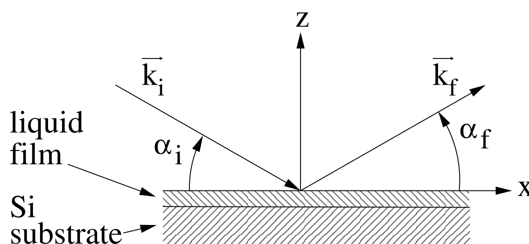

Figure 3. A sketch of the scattering geometry. The incident beam with wavevector $\vec{k}_\mathrm{i}$ hits the liquid film on top of the substrate and is reflected. The angles α_i, α_f range from 0° to approximately 5°.

The wetting films were prepared in an x-ray cell made out of a beryllium cylinder inside an aluminium vacuum cell. The inner cell contains the four silicon wafers with the wetting films. A sketch of the cell is shown in figure 4. The thermal isolation guarantees a temperature stability of $\Delta T < 2$ mK inside the inner cell over a data collection period of 75 minutes, while the temperature of the outer cell could be controlled with an accuracy of approximately 0.1 K by means of an external water circuit. The temperature stability is of decisive importance for the stability of the prepared films and thus for the reproducibility of the results. A reservoir for the liquids is thermally decoupled and placed about 2 cm below the previously evacuated x-ray cell. In the following the temperature inside the inner beryllium cell is denoted as T while the temperature of the liquids in the reservoir is denoted by T_r. The temperature T_r was constant with an accuracy better than 5 mK. The inner cell and the reservoir were evacuated through a septum using a syringe. The liquid was let into the reservoir in a similar manner after an initial measurement of the dry wafers (see above). The temperature T of the chamber containing the wafers and that of the reservoir were controlled independently using LakeShore 340 and 330 temperature controllers. Temperatures from 288 K up to 305 K were accessible. By cooling or heating the reservoir, i.e. by changing T_r, it is possible to change the vapour pressure of the injected liquids and hence the film thickness d without changing the temperature inside the x-ray cell—that is, under equilibrium conditions. With this set-up, stable films with thicknesses in the range 140 Å $< d <$ 350 Å were prepared.

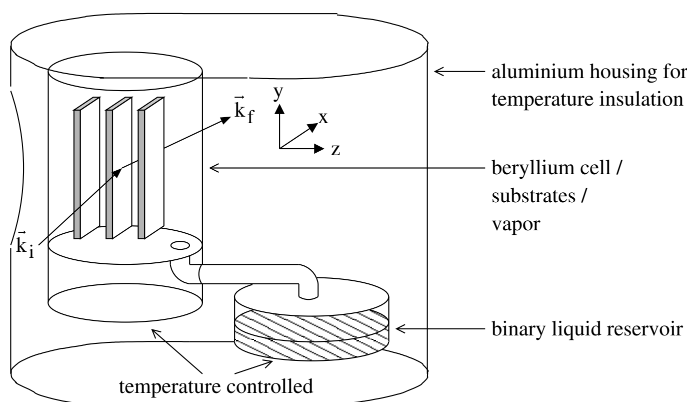

Figure 4. The set-up for measuring the x-ray scattering from a thin film of a binary liquid absorbed on a substrate. The z-direction is perpendicular to the surface of the substrate; the wavevectors $\vec{k}_f$ and $\vec{k}_i$ are in the horizontal x–z plane; y is the out-of-plane direction.

Apart from the temperature stability, the most serious problem for the investigation of liquid films with synchrotron radiation is radiation damage. Therefore all reflectivities were measured twice in order to check whether changes have occurred during the data acquisition. In addition, four wafers were mounted together inside the beryllium cell to increase the total area which is wetted by the binary mixtures. This allows a measurement of many films, each on a previously unirradiated part of the wafer, without opening the sample cell and without injections of new material (for further details of the set-up, see references [12, 47]).

5. Measurements and discussion

In order to highlight smaller features of the reflectivity data, in the following $R(q_z)/R_F(q_z)$ is always plotted, i.e. the measured reflectivity $R(q_z)$ normalized by the Fresnel reflectivity

$R_F(q_z)$ of a silicon substrate with a sharp interface. This cancels the rapid intrinsic q_z^{-4} decrease of the data due to the Fresnel formula (see equation (2)).

Figure 5 shows an example of x-ray reflectivity data for a hexane/perfluorohexane wetting film. A 1:1 by volume mixture of the two materials was injected into the sample cell. The temperatures were $T = 294$ K and $T_r = 296$ K, respectively. The line shows the reflectivity calculated assuming a single liquid layer with homogeneous density. The model clearly fails to reproduce the data in the low- and high-q_z regions. When dividing the liquid film into two films with different densities and introducing a transition region (modelled by an error function [29, 30]), good fits result after refinement with the Parratt algorithm according to equations (1)–(3). However, the high-q_z data are still not well explained. In a next step (figure 6) the inversion (see equation (6)) was applied using the fit result as the start profile. Now the agreement between the data and the calculation is almost perfect over the entire range of the experiment. The interfaces of the resulting profile were afterwards approximated by error functions where the widths of these functions are the interface or surface roughnesses of the system. All data which are given in the following have been treated with this refinement procedure.

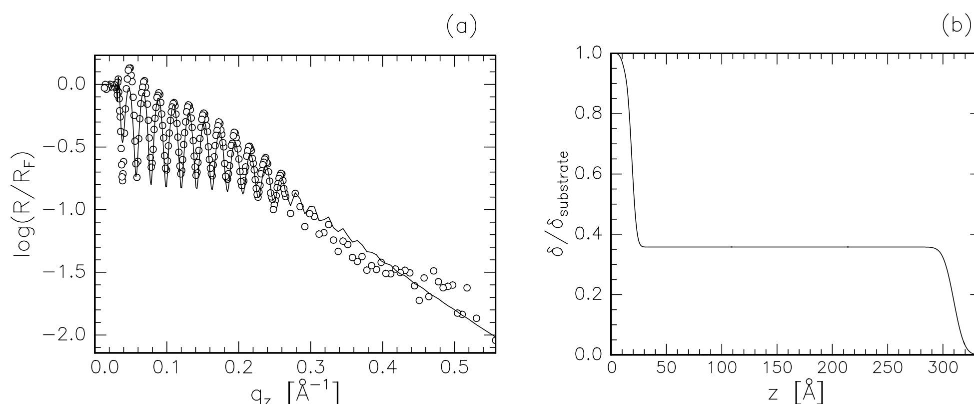

Figure 5. An example of x-ray specular reflectivity (○ (a)) and a fit (solid line) for a film with a homogeneous density profile (b).

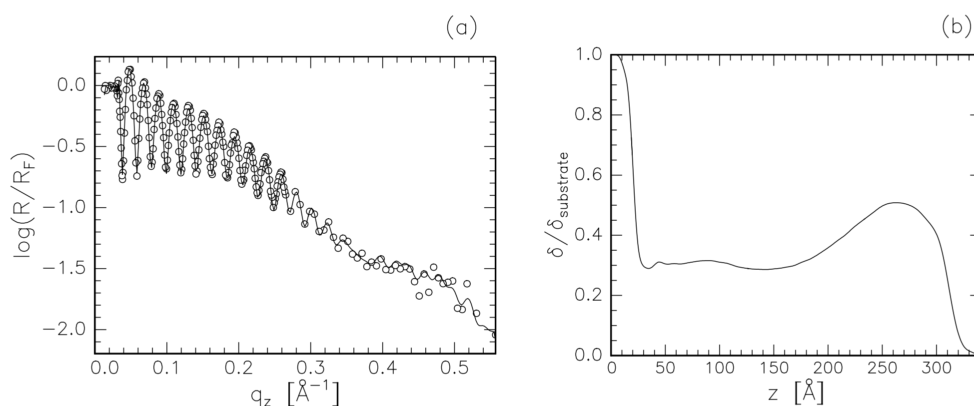

Figure 6. An example of x-ray specular reflectivity (○ (a)) and a fit (solid line) for a film with a density profile refined by inversion (b). See the text for details.

Figures 7–10 show two series of reflectivity data and the corresponding density profiles. The profiles are shown as obtained from the inversion process, without further smoothing. Some curves in figures 8 and 10 show oscillatory artifacts which stem from the Fourier transformation involved in the process. The first series (figure 8) was taken with increasing temperatures inside the inner sample cell, $T = 291, \ldots, 299$ K, while the temperature of the reservoir was always two degrees higher, i.e. $T_r = T + 2$ K. Figure 10 shows a similar series of measurements but for decreasing temperatures from $T = 299$ K to $T = 288$ K. A region of higher density at the liquid/vapour interface was found for all films. This finding is in agreement with the results of reference [30] and in agreement with molecular dynamics simulations that show an enrichment of the species with lower surface tension in an octane/butane binary

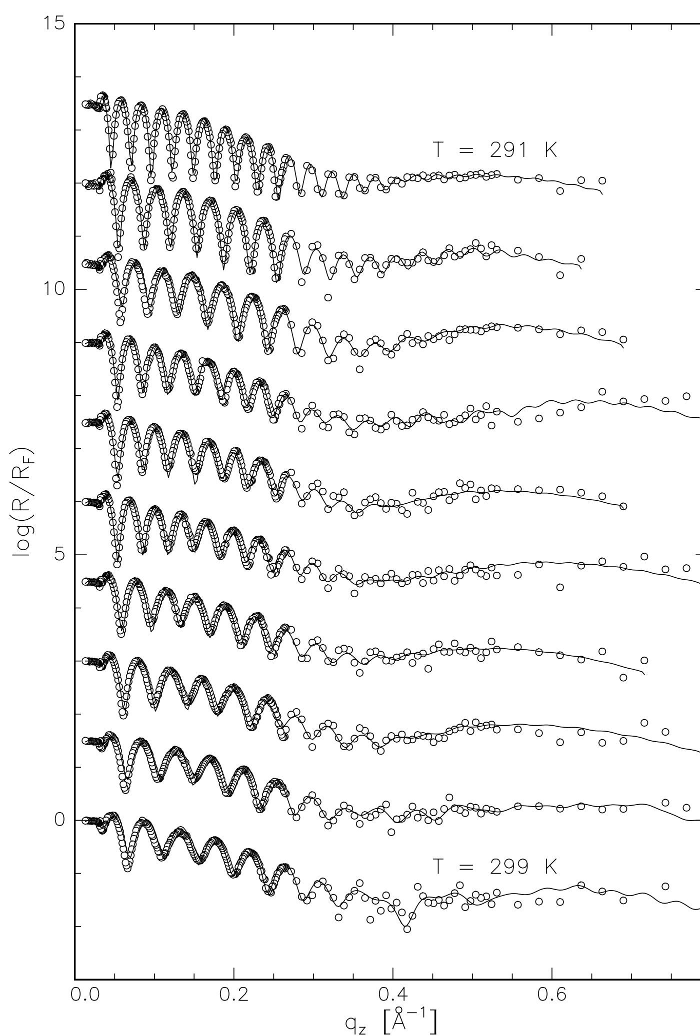

Figure 7. X-ray specular reflectivities of wetting films of a hexane/perfluorohexane mixture with liquid volume ratio 1:1 (○) in the reservoir. The data are shifted for clarity. The film temperatures are, from top to bottom: $T = 291$, 292, 293, 293.5, 294, 295, 296, 297, 298, and 299 K. The solid lines are the results of the refinements based on data inversion. The corresponding density profiles are shown in figure 8.

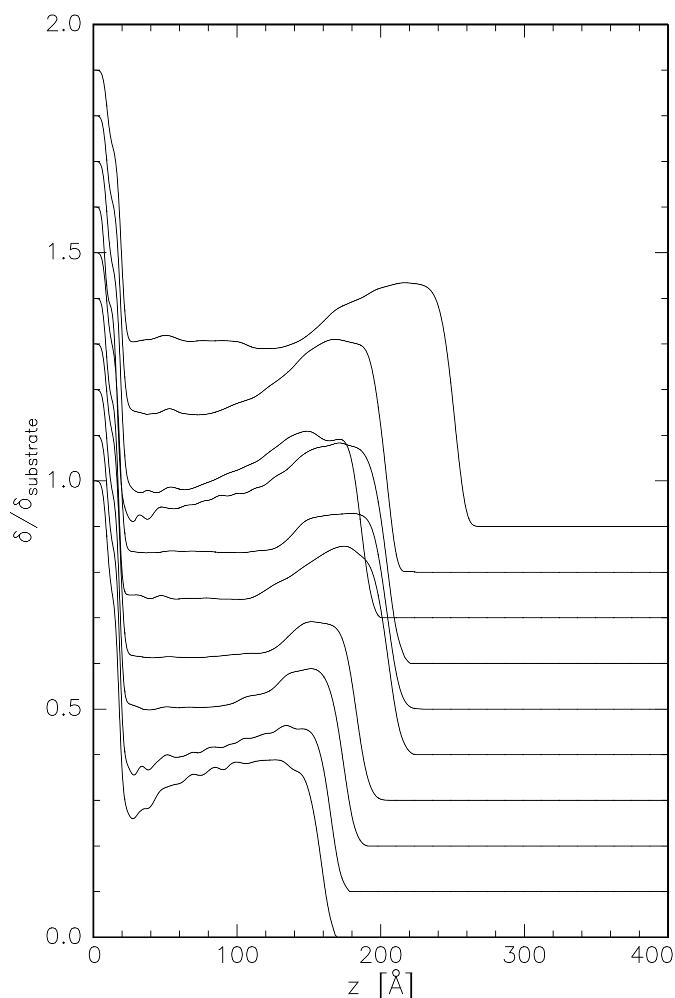

Figure 8. Density profiles corresponding to the reflectivity data shown in figure 7. The film temperatures are, from top to bottom: $T = 291$, 292, 293, 293.5, 294, 295, 296, 297, 298, and 299 K. The dispersion of bulk hexane relative to the substrate is $\delta/\delta_{\mathrm{substrate}} = 0.33$, and that of bulk perfluorohexane is $\delta/\delta_{\mathrm{substrate}} = 0.69$. The profiles are shifted for clarity.

film [48]. It is worth noting that even in the one-phase region of the bulk phase diagram ($T \geqslant 296$ K in figures 8 and 10), the film is apparently still in the two-phase region.

Figures 11–15 show the results for several film parameters, which were extracted from the film profiles. The temperatures T are always in the vicinity of the temperature $T_c = 295.2$ K of the bulk critical point. The film thickness d is shown in figure 11. While the thickness d of a measured film can be determined with high accuracy ($\Delta d < 2$ Å), its value apparently depends on the local substrate conditions. Because of radiation damage, each measurement was done on a different substrate position. Hence, there is some scatter of the data. Taking this into account, we find a continuous variation of the film thickness with T. With increasing temperatures from 291 to 299 K the thickness decreases ($\circ$). The curve for decreasing temperatures has been measured for a different wafer, where somewhat higher film thicknesses were obtained ($\bullet$). However, the two curves give the same trend.

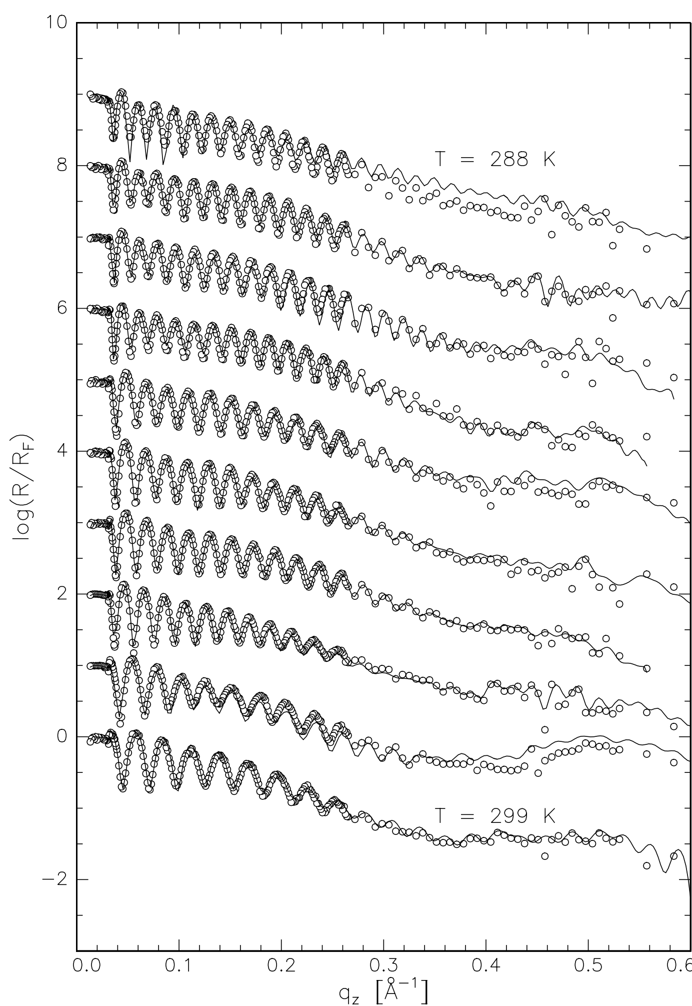

Figure 9. X-ray specular reflectivities of wetting films of a hexane/perfluorohexane mixture with liquid volume ratio 1:1 (○) in the reservoir. The data are shifted for clarity. The film temperatures are, from bottom to top: $T = 299$, 297, and then 295, 294, . . ., 288 K. The solid lines are the results of the refinement based on data inversion. The corresponding profiles are shown in figure 10. For $q_z > 0.55$, the intensity approaches the background level and yields little information.

The film profiles show a pronounced local maximum δ_{max} of the dispersion near the surface of the film, and a minimum δ_{min} is found in the region closer to the substrate. These values may be converted into local concentrations of perfluorohexane $c_{\text{p.f.,max}}$ and $c_{\text{p.f.,min}}$ assuming a linear interpolation $\delta = \delta_{\text{hex}}(1 - c_{\text{p.f.}}) + \delta_{\text{p.f.}} c_{\text{p.f.}}$. The resulting data are shown in figure 12. If a phase transition had taken place in the system, it would show up here, since particularly changes of δ_{max} or δ_{min} are expected at the consolute line. However, the scatter of the data exceeds the marked systematic changes of the curves. For temperatures below $T_{\text{c,bulk}} = 295.2$ K, a tendency to higher $c_{\text{p.f.,max}}$ is clearly visible, whereas the minimum concentration is always about $c_{\text{p.f.,min}} = 0 \pm 0.2$, indicating that a part of the film always has the density of nearly pure hexane. The second (weaker) density maximum that some films show between the substrate and the surface maximum (see figure 10) is not yet understood.

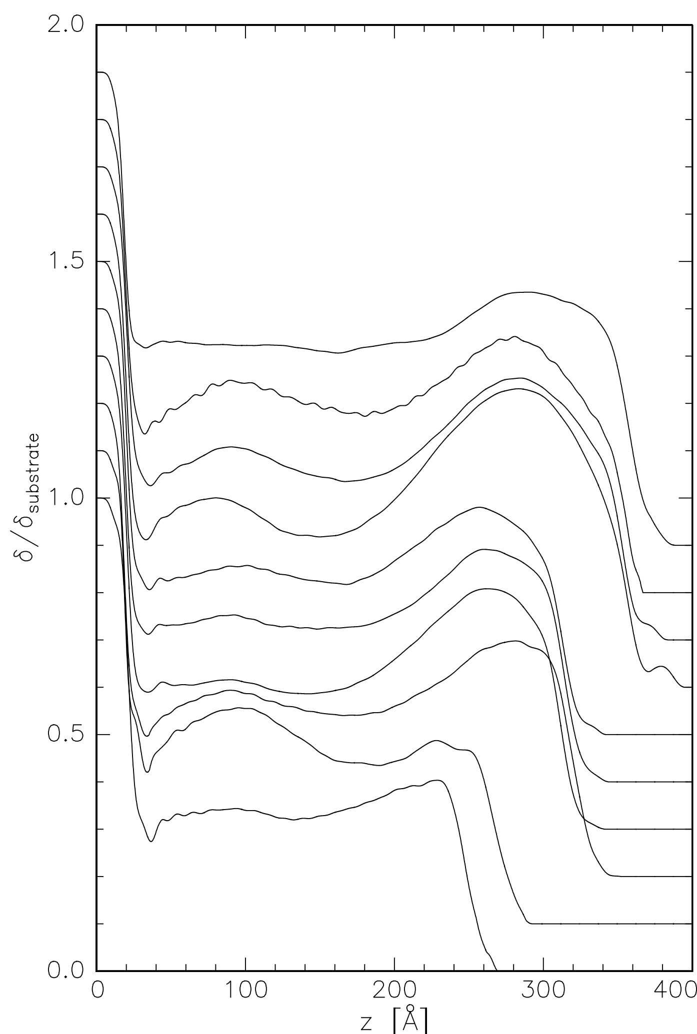

Figure 10. Density profiles corresponding to the reflectivity data shown in figure 9. The film temperatures are, from bottom to top: $T = 299, 297$, and then $295, 294, \ldots, 288$ K. The dispersion of bulk hexane relative to the substrate is $\delta/\delta_{\mathrm{substrate}} = 0.33$, and that of bulk perfluorohexane is $\delta/\delta_{\mathrm{substrate}} = 0.69$. The profiles are shifted for clarity.

Figure 13 shows the position of the inner interface of the film, given in units of the film thickness d. The position $z_{\mathrm{interface}}/d$ changes from 0.61 to 0.75 with little scatter. There seems to be a systematic tendency for the perfluorohexane-enriched part of the film to reduce with increasing temperature. Rather speculatively, from an extrapolation, a transition to a single-phase film may be anticipated at $T = 315 \pm 10$ K. Doing the same extrapolation with the data from figure 12, one reaches convergence of the maximum and minimum concentrations at $T = 303 \pm 5$ K. An integration of the liquid film profile (after subtracting the substrate part) shows that the mean density of the film decreases with increasing temperature towards the density of pure hexane. This is the same trend as is derived from figures 12 and 13.

Figure 14 shows a sketch of the path in the density–temperature diagram (determined from the mean film densities) in comparison to the bulk phase diagram from [29] (see the materials

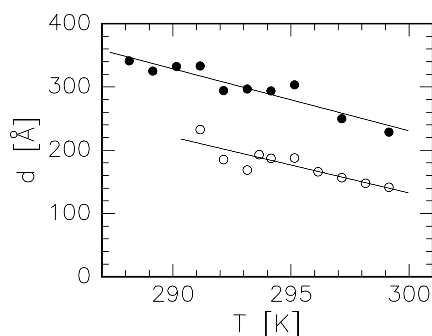

Figure 11. Thickness of the liquid films, measured in the order of increasing temperature (series 1, ○) and decreasing temperature (series 2, •). The values were extracted from the density profiles shown in figures 8 and 10. The lines are guides to the eye, only.

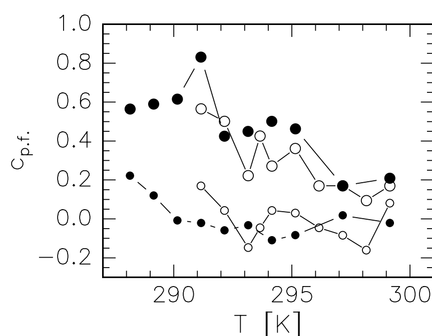

Figure 12. Maximum (big symbols) and minimum (small symbols) concentration $c_{\mathrm{p.f.}}$ of perfluorohexane in the liquid films, measured in order of increasing temperatures (series 1, ○) and decreasing temperatures (series 2, •). The lines are guides to the eye, only. The values were extracted from the density profiles shown in figures 8 and 10; details are explained in the text. At 297 K in series 2, unlike for the other measurements, the global concentration maximum of the liquid film was located near the substrate and not near the surface. Here the local concentration maximum near the film surface is shown for comparison.

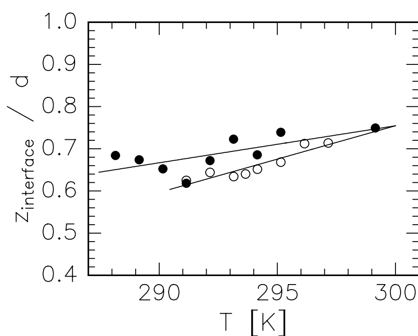

Figure 13. Relative position of the inner interface inside the films, measured in the order of increasing temperatures (series 1, ○) and decreasing temperatures (series 2, •). The lines are guides to the eye, only. The values were extracted from figures 8 and 10, wherever an interface was clearly detectable.

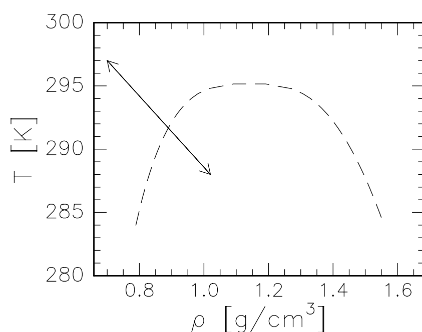

Figure 14. A sketch of the path in the density–temperature diagram, determined from the mean density of the films shown in figures 8 and 10 (solid line). The bulk consolute line is shown for comparison (dashed line) [29].

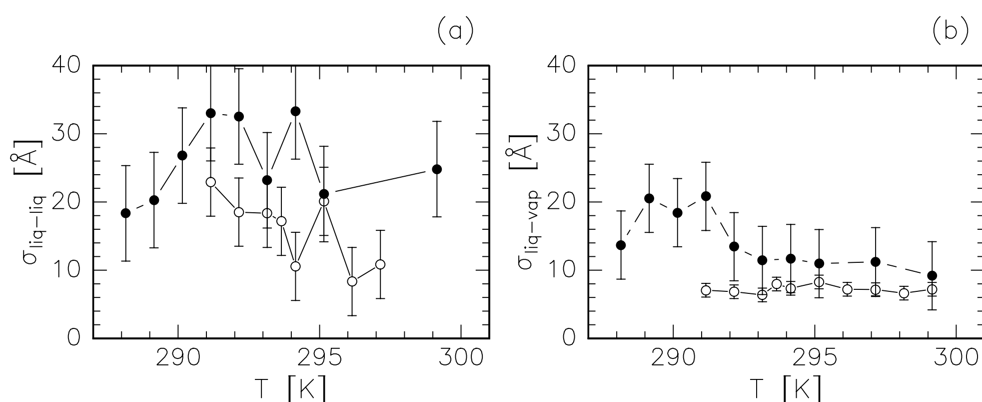

Figure 15. Roughnesses of the liquid–liquid (a) and liquid–vapour interfaces (b) of the films shown in figures 9 and 11, displayed for series 1 with increasing temperatures (○) and series 2 with decreasing temperatures (●).

section above). The diagram shows that the bulk consolute line was crossed in the temperature series of figures 8 and 10, and that the transition from the bulk two-phase region to the one-phase region (with increasing temperature) and back again (with decreasing temperature) was expected in the parameter range investigated even though at lower density and temperature than at the bulk critical point (T_c, ρ_c). Our measurements show that the bulk phase diagram does not describe the mixing behaviour in the thin liquid films without modification. A likely explanation is that the consolute line has shifted towards higher temperatures. But still the measured film behaviour differs from the bulk mixing phenomenon in the sense that the thin-film system drastically changes its composition due to material exchange with the vapour.

Finally, figure 15 shows the roughnesses of the film interfaces for the series with increasing (○) and decreasing (●) temperatures. Displayed are the fitted roughness of the inner film interface $\sigma_{\mathrm{liq-liq}}$ (ranging from 8 to 34 Å, (a)), and that of the free surface of the film $\sigma_{\mathrm{liq-vap}}$ (ranging from 6 to 20 Å, (b)). The substrate roughness is always about 2–4 Å and is not shown. A calculation of surface roughnesses for films of pure hexane or perfluorohexane [12] yields values of $\sigma_{\mathrm{liq-vap}} \approx 7$ Å–10 Å for a similar range of temperatures and film thicknesses. This is comparable with the values measured for the series with increasing temperatures, but does not explain the much higher roughnesses of the series taken at decreasing temperatures. The

roughnesses of the liquid–liquid interface are much smaller than what has been measured for the bulk system at criticality, where the interfacial width grows from 60 Å at 288 K to 210 Å at 294 K [29]. We have no calculations for the width of the liquid–liquid interface in the thin films. As for the bulk system, one would expect a broadening of the interface on approaching the transition to a single-phase system, with the two subfilms becoming more similar and the interface tension smaller, but the data do not show this tendency.

6. Conclusions and outlook

Thin wetting films of a mixture of hexane and perfluorohexane have been investigated by x-ray specular reflectivity measurements. For temperatures in the range of 291 to 299 K, an enrichment of perfluorohexane at the surface of the films is found. This is in qualitative agreement with molecular dynamics simulations for a butane/octane system [48]. The temperature dependence of the demixing behaviour of binary films differs from the well-known bulk mixing behaviour in two respects:

(i) The films seem to remain in the two-phase region even for temperatures several degrees higher than $T_{\mathrm{c,bulk}}$. Here an elaboration on the influence of substrate effects, e.g. those found in pure hexane films [14, 15], could shed light on the classification of the film profile as describing a one-phase or a two-phase film.
(ii) On variation of the temperature, the molecules are not simply redistributed within the film (as in the bulk system); the composition of the film varies due to material exchange with the vapour.

Acknowledgments

This work was supported by the Deutsche Forschungsgemeinschaft projects Pr325/10-1 and Pr325/10-2 within the Schwerpunktprogramm 'Benetzung und Strukturbildung an Grenzflächen'. We thank Dr D Novikov (HASYLAB) for help during the experiments and Dr P Dreier (Wacker Siltronic, Burghausen) for providing the high-quality silicon substrates.

References

[1] Ebner C and Saam W F 1977 *Phys. Rev. Lett.* **38** 1486
[2] Plischke M and Henderson D 1986 *J. Chem. Phys.* **84** 2846
[3] Götzelmann, B, Haase A and Dietrich S 1996 *Phys. Rev.* E **53** 3456
[4] Krämer A, Vossen M and Forstmann F 1997 *J. Chem. Phys.* **106** 2792
[5] Granick S 1999 *Phys. Today* **52** (7) 26
[6] Ribarsky M W and Landman U 1992 *J. Chem. Phys.* **97** 1937
[7] Gao J, Luedtke W D and Landman U 1997 *J. Chem. Phys.* **106** 4309
[8] Hentschke R and Winkler R G 1993 *J. Chem. Phys.* **99** 5528
[9] Winkler R G, Schmid R H, Gerstmaier A and Reineker P 1996 *J. Chem. Phys.* **104** 8103
[10] Huisman W J, Peters J F, Zwanenburg M J, de Vries S A, Derry T E, Abernathy D and van der Veen J F 1997 *Nature* **390** 397
[11] Yu C-J, Richter A G, Datta A, Durbin M K and Dutta P 1999 *Phys. Rev. Lett.* **82** 2326
[12] Doerr A K 1999 *PhD Thesis* Kiel University
[13] Doerr A K, Tolan M, Prange W, Schlomka J-P, Seydel T, Press W, Smilgies D and Struth B 1999 *Phys. Rev. Lett.* **83** 3470
[14] Doerr A K, Tolan M, Seydel T and Press W 1998 *Physica* B **248** 263
[15] Doerr A K, Tolan M, Schlomka J-P and Press W 2001 *Europhys. Lett.* **52** 330
[16] Magnussen O M, Ocko B M, Regan M J, Penanen K, Pershan P S and Deutsch M 1995 *Phys. Rev. Lett.* **74** 4444

[17] Regan M J, Kawamoto E H, Lee S, Pershan P S, Maskil N, Deutsch M, Magnussen O M, Ocko B M and Bermann L E 1995 *Phys. Rev. Lett.* **75** 2498
[18] Getta T and Dietrich S 1993 *Phys. Rev.* E **47** 1856
[19] Narayanan T and Kumar A 1994 *Phys. Rep.* **249** 135
[20] Diehl H W and Ciach A 1991 *Phys. Rev.* B **44** 6642
[21] Diehl H W and Smock M 1993 *Phys. Rev.* B **47** 5841
[22] Flöter G and Dietrich S 1995 *Z. Phys.* B **97** 213
[23] Liu A J and Fisher M E 1989 *Phys. Rev.* A **40** 7202
[24] Diehl H W 1986 *Phase Transitions and Critical Phenomena* vol 10, ed C Domb and J L Lebowitz (London: Academic) p 75
[25] Schlossman M, Wu X-L and Franck C 1985 *Phys. Rev.* B **31** 1478
[26] Dixon J A, Schlossman M, Wu X-L and Franck C 1985 *Phys. Rev.* B **31** 1509
[27] Zhao H, Penninckx-Sans A, Lee L-T, Beysens D and Jannink G 1995 *Phys. Rev. Lett.* **75** 1977
[28] Plech A, Klemradt U, Huber M and Peisl J 2000 *Europhys. Lett.* **49** 583
[29] McClain B M, Yoon M, Lister J D and Mochrie S G J 1999 *Eur. Phys. J.* B **10** 45
[30] Heilmann R, Fukuto M and Pershan P S 2001 *Preprint*
[31] Mukhopadhyay A and Law B M 1999 *Phys. Rev. Lett.* **83** 772
[32] Bedford R G and Dunlop R D 1958 *J. Am. Chem. Soc.* **80** 282
[33] Daillant J and Gibaud A (ed) 1999 *X-Ray and Neutron Reflectivity (Springer Lecture Notes in Physics vol 58)* (Berlin: Springer)
[34] Holý V, Pietsch U and Baumbach T 1999 *X-Ray Scattering from Thin Films (High Resolution X-Ray Scattering from Crystalline Thin Films) (Springer Tracts in Modern Physics vol 149)* (Berlin: Springer)
[35] Tolan M 1999 *X-Ray Scattering from Soft-Matter Thin films—Materials Science and Basic Research (Springer Tracts in Modern Physics vol 148)* (Berlin: Springer)
[36] *Handbook of Chemistry and Physics* 1995–1996 76th edn, ed D R Lide (Boca Raton, FL: Chemical Rubber Company Press)
[37] Born M and Wolf E 1993 *Principles of Optics* (Oxford: Pergamon)
[38] Parratt L G 1954 *Phys. Rev.* **95** 359
[39] Abelès F 1950 *Ann. Phys., Paris* **5** 596
[40] Sanyal M K, Sinha S K, Gibaud A, Huang K G, Carvalho B L, Rafailovich M, Sokolov J, Zhao X and Zhao W 1993 *Europhys. Lett.* **21** 691
[41] van der Lee A 2000 *Eur. Phys. J.* B **13** 755
[42] Sanyal M K, Basu J K, Datta A and Banerjee S 1996 *Europhys. Lett.* **36** 265
[43] Sanyal M K, Hazra S, Basu J K and Datta A 1998 *Phys. Rev.* B **58** R4258
[44] Zimmermann K-M, Tolan M, Weber R, Stettner J, Doerr A K and Press W 2000 *Phys. Rev.* B **62** 10 377
[45] Als-Nielsen J, Jacquemain D, Kjær K, Leveiller F and Lahav M 1994 *Phys. Rep.* **246** 251
[46] Seeck O H, Kaendler I D, Tolan M, Shin K, Rafailovich M H, Sokolov J and Kolb R 2000 *Appl. Phys. Lett.* **76** 2713
[47] Prange W 2001 *PhD Thesis* Kiel University
[48] Smith P, Lynden-Bell R M and Smith W 2000 *Mol. Phys.* **98** 255